Simulation of ^{252}Cf Neutron Transmission Through an Iron Sphere

Mario Matijević, Krešimir Trontl, Dubravko Pevec
University of Zagreb, Faculty of Electrical Engineering and Computing,
Department of Applied Physics
Unska 3, 10000 Zagreb, Croatia
mario.matijevic@fer.hr, kresimir.trontl@fer.hr, dubravko.pevec@fer.hr

ABSTRACT

This paper presents an extension of an earlier study to test iron cross-section data from ENDF/B-VII.1 library to be used in Monte Carlo and transport calculations of neutron transmission through an iron sphere. Deficiencies in the iron inelastic data from the previous ENDF/B-V evaluation was a known issue, giving concern for a fast neutron flux underestimation within the reactor pressure vessels. In order to benchmark the next-generation ENDF/B-VI iron data, the U.S. Nuclear Regulatory Commission and the former Czechoslovakian National Research Institute have jointly preformed several experiments in 1990s, addressing neutron leakage spectra obtained for a ^{252}Cf fission source in a centre of an iron sphere. It was shown that the ENDF/B-VI iron cross section, containing several improvements over previous evaluations, will not entirely resolve the neutron spectrum discrepancies observed at high neutron energies. Since safety analyses of reactor pressure vessel embrittlement are often based on neutron transport calculations using specific multigroup cross section libraries, simulation of this benchmark was performed using a hybrid shielding methodology of ADVANTG3.0.3/MCNP6.1.1b codes. Comparison of calculated and referenced dosimeter activation rates are presented for several "standard" nuclear reactions, often used in reactor pressure vessel dosimetry. For that purpose, the new IRDFF-II special library was used as a reference source of dosimetry cross sections. The MCNP6.1.1b computed reaction rates were also analysed using previous IRDFF-1.05 special library and general purpose ENDF/B-VII.1 library.

Keywords: *dosimetry, shielding, Monte Carlo, MCNP, ADVANTG*

1 INTRODUCTION

Prior to release of ENDF/B-VI evaluation there has been a reasonable concern that deficiencies in the iron inelastic scattering data may cause an underestimation in the calculated fast neutron flux within the reactor pressure vessels (RPVs) of power reactors [1]. At that time most of the USA safety analyses of RPV embrittlement were based on transport calculations with multigroup energy structure for obtaining fast neutron fluence inside the vessel regions. Validation of such transport solutions with measured dosimeter activation rates in the ex-vessel cavity region often indicated underestimation of calculated fast flux by up to 30% [1], directly influencing expectation value for reactor operational lifetime. With the release of ENDF/B-VI some 30 years ago, an improvement in iron evaluations for cross sections above 1 MeV came along with the following: 1) correlation between incident neutron energy and forward bias in the angular distribution for inelastic scattering; 2) a reduction in the magnitude of the inelastic cross section data in the fast neutron region. Initial data testing of the ENDF/B-VI iron data was done by Williams et al [2], but resulting in large discrepancies of measured and calculated neutron leakage

spectra above 1 MeV from an iron sphere containing deuterium-tritium source of neutrons with 14.1 MeV. Clear conclusions of that experiment were not reached, except that interaction of 14.1 MeV neutrons in iron were quite different compared to moderated fission spectrum incident on RPV of commercial plants. This difficulty was overcome in the next phase of benchmarking the ENDF/B-VI iron data described by Sajo et al [1] using a new experimental configurations. The U.S. NRC and the former Czechoslovakian National Research Institute (NRI) in Rež (Czech Republic) have jointly conducted calculation and measurement of neutron leakage spectra from a ^{252}Cf fission source located at the centre of an iron sphere. The spontaneous fission spectrum of ^{252}Cf is similar to a hardened ^{235}U fission spectrum but without the 1/*E* slowing-down component, important for low energy threshold dosimeters. The paper [1] gives detailed comparison of calculated and experimental results, with major finding that the ENDF/B-VI cross sections improve fast neutron transmission through iron, but at the same time will not entirely resolve the neutron spectrum underestimation compared to experimental data for neutron energies above 1 MeV.

This paper presents revision of this research using modern computational tools. The Monte Carlo (MC) simulation of fast neutron transmission through an iron sphere was performed for the dual purpose: 1) testing of iron transport cross section data contained in the general purpose ENDF/B-VII.1 cross section library [3] and direct comparison with older ENDF/B-VI evaluation; 2) testing special dosimetry libraries IRDFF-II [4] and IRDFF-1.05 [5] with several reactions covering thermal, epithermal and fast neutron region to be used as a response functions on point detector 1 m away from the centre of the iron sphere. This paper is organized as follows. Section 2 gives the experimental description and original calculations. The computational tools ADVANTG/MCNP are given in Section 3, together with a simulation model description. Section 4 gives results and discussion, while Section 5 gives conclusions. The referenced literature is given at the end of the paper.

2 EXPERIMENTAL DESCRIPTION AND ORIGINAL CALCULATIONS

The original set of experiments was performed using iron spheres of various sizes with small ^{252}Cf source located at the geometrical centre. The reference paper [1] and this paper are analysing one specific case, which is an iron sphere with an outer radius of 25 cm. Two independent measurements (NRI and Skoda Company) of the fast neutrons leaking from the surface of the iron sphere were done using a proton-recoil detector and a stilbene crystal spectrometer located at 100 cm from the source. No detailed information about the detector configuration was provided in paper [1], but schematic diagram of experimental setup and central section of the source were included and are depicted here in Figure 1 and Figure 2 for the purpose of completeness.

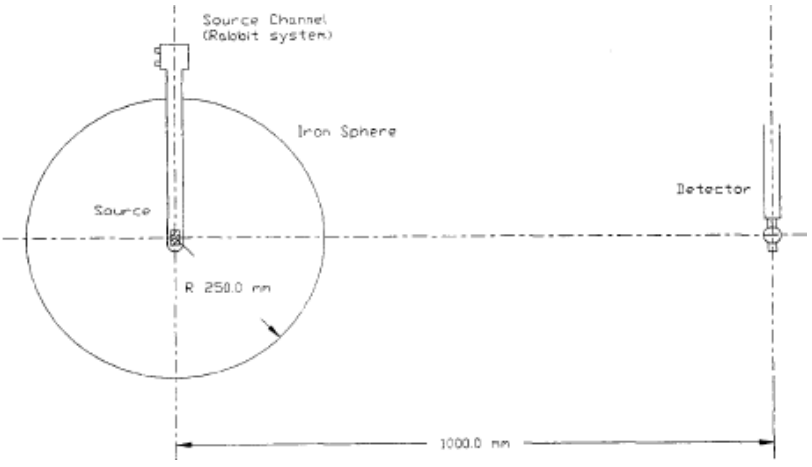

Figure 1: Experimental setup for iron sphere and point detector [1]

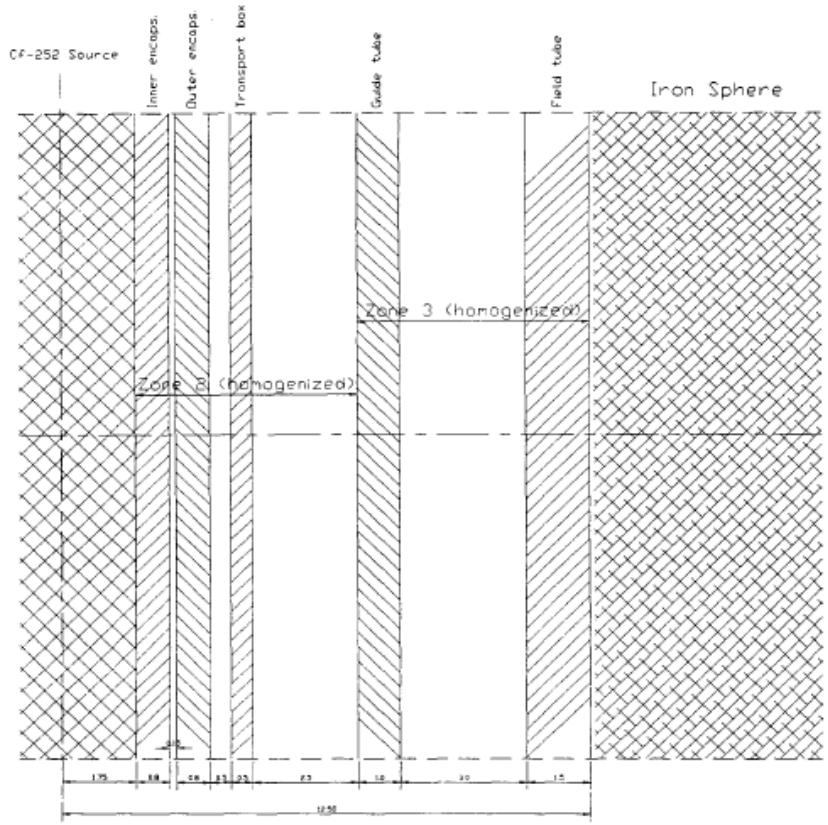

Figure 2: Enlarged central section of the rabbit system housing the ^{252}Cf source [1]

The safe handling of the neutron source is achieved by the so-called rabbit system, which consists of two concentric cylindrical tubes, movable guide tube inside a fixed field tube. The tubes and transport box enclosing the source are made from aluminium alloy. The ^{252}Cf source is in a form of cylinder with 0.35 cm in diameter and 1.2 cm in height and has a double stainless steel encapsulation. The dimensions of rabbit system tubes, transport box, steel encapsulation and cylindrical source can be found in [1] with material compositions of various elements.

The reported neutron transport calculations were done using the one-dimensional discrete ordinates (SN) computer code XSDRNPM-S in a spherical geometry. For that purpose, the central cylindrical region of the experimental configuration was modelled as three separate homogenized spherical zones: Zone 1 containing the source (void region); Zone 2 containing source encapsulation and transport box; Zone 3 capturing the rabbit system. The spherical symmetry throughout the model geometry thus comprises of iron shield with inner radius of 1.25 cm and outer radius of 25 cm. The SN mesh interval size was 0.16 cm with S16/P3 parameters taken for quadrature set and Legendre expansion of the scattering cross sections. The calculations were performed using 174 energy groups with the new ENDF/B-VI iron data while keeping cross sections of other material unchanged, i.e. from previous evaluation. The resonance self shielding calculations based on Bondarenko method were performed with the computer program BONAMI-S. The fission spectrum of ^{252}Cf source was used from the National Institute of Standards and Technology (NIST), but without additional details. The source strength was normalized to produce a neutron flux value of 1 n/cm^2/s at the location of point detector (r=100 cm) without the iron shield giving in turn 125664 n/s. The computed neutron leakage spectrum at detector location enabled calculation of various reaction rates (i.e. integral responses) for different threshold detectors, while reactions of interest presented in Table 1 are typical for RPV dosimetry.

Table 1: Evaluated integral responses

Reaction of interest	Threshold energy (MeV)
63Cu(n,α)	4.7
54Fe(n,p)	2.3
58Ni(n,p)	2.1
238U(n,f)	1.5
237Np(n,f)	1.2
59Co(n,g)	thermal

These reactions of interest were used as a neutron response functions in transport calculations of dosimeter reaction rates and were originally processed from the ENDF/B-V dosimetry file. The VITAMIN-E cross section library also contains these reactions and it was mentioned how the ^{63}Cu(n,α) cross section is known to be too large [1].

3 CALCULATIONAL METHOD

The hybrid shielding computer programs ANDVANTG/MCNP use a deterministic transport solver Denovo [6] as a means for automatic, adjoint and mesh-based variance reduction (VR) generation. With such VR parameters the final optimized MC calculation is done. The Denovo is implementing Consistent Adjoint Driven Importance Sampling (CADIS) and Forward Weighted CADIS (FW-CADIS) methodologies [7], developed at Oak Ridge National Laboratory (ORNL). It is a very fast and robust SN solver, working with structured Cartesian grid and based on the Koch-Baker-Alcouffe parallel transport sweep algorithm across x-y domain blocks. The most important feature is multigroup flux positivity when using Step Characteristic (SC) spatial differencing option which is basis for numerical stability of final MC simulation.

3.1 MCNP/ADVANTG hybrid shielding methodology

The ADVANTG3.0.3 [8] is an automated tool for generating variance reduction parameters for fixed-source continuous-energy Monte Carlo simulations with MCNP code, based on approximate 3D multigroup discrete ordinates adjoint transport solutions [9][10] generated by Denovo. The VR parameters generated by ADVANTG consist of space-energy dependent weight-window bounds (WW) and biased source distributions, which are outputted in formats that can be directly used with MCNP input. ADVANTG has been applied to neutron, photon, and coupled neutron-photon simulations of real-world radiation detection and shielding scenarios. ADVANTG is compatible with all MCNP geometry features and can be used to accelerate cell tallies (F4, F6, F8), surface tallies (F1 and F2), point-detector tallies (F5), and Cartesian mesh tallies (FMESH). The solution methods of ADVANTG are CADIS/FW-CADIS for generating VR parameters which provide a prescription for generating space-energy dependent WW targets and a consistent biased source distribution (SB cards in SDEF and WWINP file). The CADIS method was developed for accelerating individual tallies, whereas FW-CADIS can be applied to multiple tallies and mesh tallies.

The MCNP6.1.1b [11] is a general-purpose Monte Carlo N-Particle code that can be used for neutron, photon, electron, or coupled neutron/photon/electron transport. The MCNP treats an arbitrary three-dimensional configuration of materials in geometric cells bounded by first- and second-degree surfaces and fourth-degree elliptical tori. For neutrons, all reactions given in a particular cross-section evaluation (such as ENDF/B-VI) are accounted for. Thermal neutrons are described by both the free gas and $S(\alpha,\beta)$ models. Important standard features that make MCNP very versatile and easy to use include a powerful general source, criticality source, and surface source; both geometry and output tally plotters; a rich collection of variance reduction techniques; a

flexible tally structure; and an extensive collection of cross-section data. Energy ranges are taken from 10^{-5} eV to 20 MeV for neutrons with data up to 150 MeV for some nuclides, 1 keV to 1 GeV for electrons, and 1 keV to 100 GeV for photons. Pointwise cross-section data were used within MCNP: auxiliary program MAKXSF prepares cross-section libraries with Doppler broadening.

3.2 MCNP simulation model description

The MCNP simulation model is based on data available in reference [1] and is presented next. The neutron source inside double steel encapsulation, transport box, rabbit system and material isotopic concentrations are taken with reported values, while several approaches were investigated for detector objects. Since no details exist on detector casing, the most basic approach was with point detector tally (F5) at location (100, 0, 0). This, however, puts more stringent statistical requirements on MC neutron flux convergence and loses advantage of inherent problem symmetry (i.e. smaller figure of merit factor), so extra verification was performed with surface flux tally (F2) and volume flux tally (F4) as thin spherical shell, both with radius of 100 cm. The axial cross sections of model geometry (y=0 plane) are depicted in Figure 3, while close-up view of the rabbit system housing the ^{252}Cf source is depicted in Figure 4.

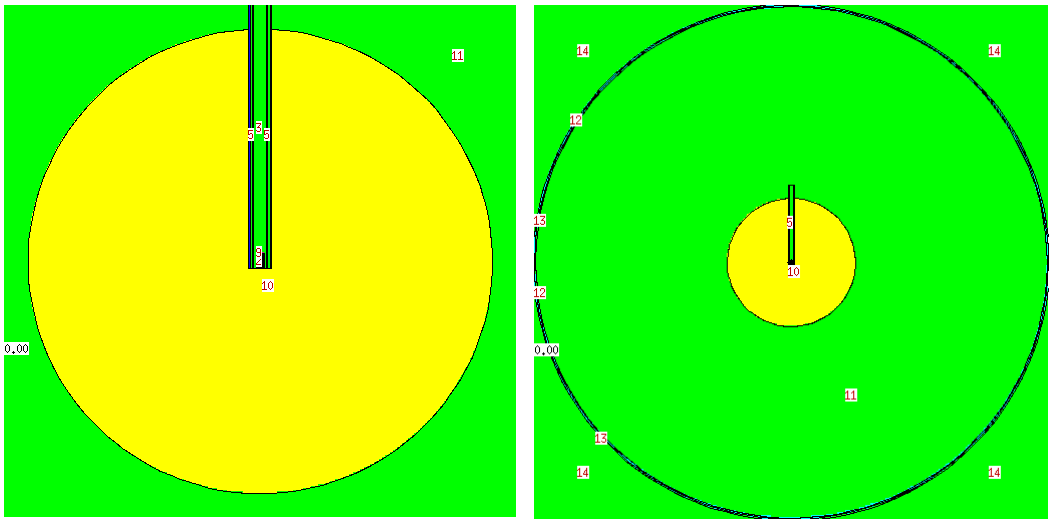

Figure 3: Iron sphere with rabbit system and distant spherical detector (yellow-iron, green-air)

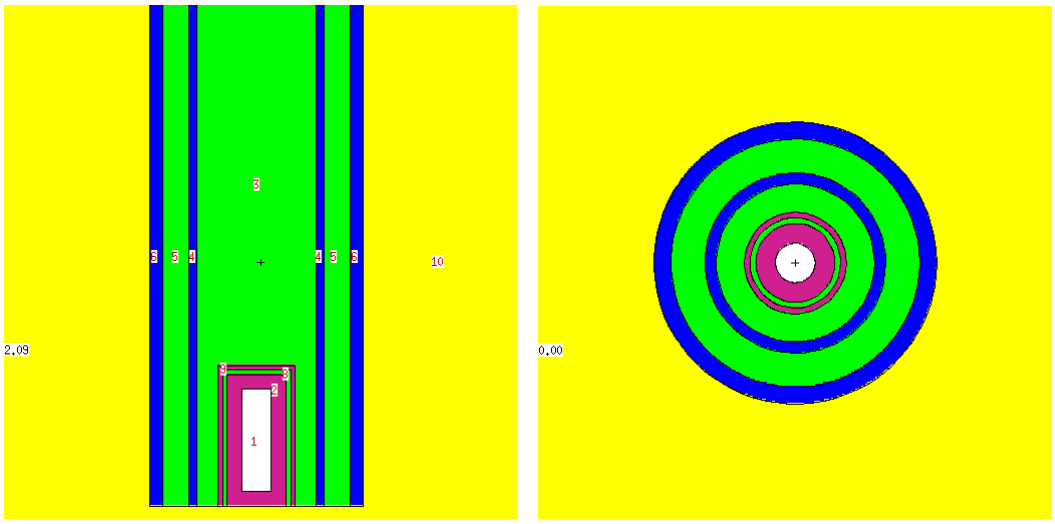

Figure 4: Axial and radial view of the rabbit system (yellow-iron, green-air, blue-steel for tubes, purple-steel for encapsulation, white-source region)

As reported in [1], the source material is modelled as cylindrical void region (depicted in white), so to achieve a proper MC sampling, MCNP source card was defined with three independent distribution functions: radial, axial and energy. For the source energy spectrum, the MCNP built-in Watt fission spectrum of ^{252}Cf with parameters a = 1.025 MeV and b = 2.926 MeV^{-1} were replaced with binned energy structure for energy biasing, so final structure was 100 equiprobable bins below 6 MeV and 28 uniform bins above 6 MeV.

The neutron transport mode was the only one allowed with "mode n" option so no secondary particles were banked. Total number of neutron histories per run was 100 million. The tallies in MCNP are always normalized to have value for 1 n/s, while true source intensity of 125664 n/s was used for proper neutron spectrum scaling and comparison with referenced values. The "FM" tally card was used to define multiplier set with a proper selection of units (barns to 1e-24 cm^2), dosimetry cross sections for response functions and MT numbers for selecting reaction type. This basically allows calculation of product between neutron flux and response function in integral fashion over tally energy structure.

Some point detectors without "FM" card were used only for monitoring a fast neutron flux over different energy regions, by using an "En" card, which also allowed comparison with referenced data. Only one point detector tally had extra fine energy group structure (about 320 groups) to capture neutron flux spectrum with fine enough resolution. As already stated, this approach with point detectors was verified with surface flux tallies and volume flux tallies. Finally, mesh tally object ("FMESH" card) was also defined to give user a sense of global MC convergence and distribution of relative errors throughout the iron sphere to detector locations. The MC mesh has 110x110x110 cells with cell side of 2 cm.

3.3 ADVANTG model description

The ADVANTG computer program is based on discrete ordinates adjoint transport solver Denovo, so only a minimal set of typical SN input blocks is needed in conjunction with the MCNP input file. Based on approximate SN flux solution, the VR parameters are developed that work in tandem and consist of space-energy dependent weight windows and biased source distributions. ADVANTG automatically modifies "SB" cards in the "SDEF" definition part of the MCNP input and provides an external file WWINP which is read during the MC simulation.

In this case ADVANTG was used with CADIS method to optimize solution of neutron flux in a single localized tally object located 75 cm away from an iron sphere surface. For that purpose, a point detector with different response functions was used and verified with alternate surface flux tally and surface shell volume tally. The ANISN-based multigroup library "bplus" was used with 47n/20g energy structure. The SN mesh was with 110x110x110 cells with 2 cm cell side and ray tracing algorithm mapped materials onto mesh cells with standard macromaterial option. Spatial discretization was step characteristic with S4/P1 parameters and diagonal transport correction for scattering cross section. Number of Krylov vectors for subspace GMRES solver was 20, maximum number of multigroup iteration was set to 100 while tolerance value was lowered to 10^{-6}. After successful run, besides generated VR parameters, ADVANTG provides very useful *.silo files to inspect quality of the SN solution with VisIt code. For example, Figure 5 shows SN solution of the adjoint flux (left) and corresponding neutron weights (right) for the first group in 47n/20g. One can clearly notice inverse relationship which is prescribed by CADIS method.

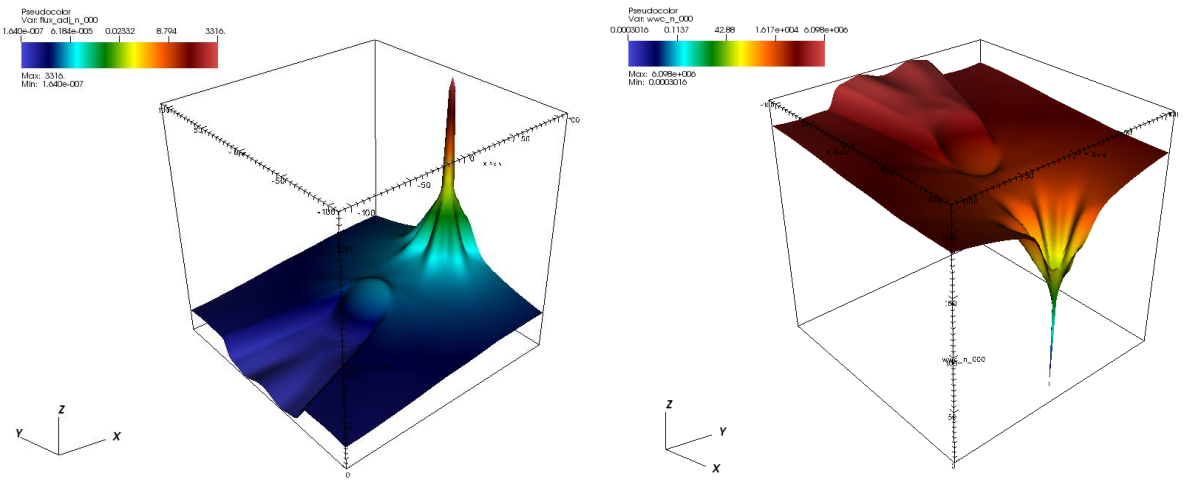

Figure 5: Adjoint flux and neutron weights in the first group of the "bplus" library

3.4 IAEA Reactor Dosimetry Files

The new International Reactor Dosimetry and Fusion File (IRDFF-II) addresses neutron dosimetry needs for fission and fusion applications for incident neutron energies from 0 to 60 MeV. The library includes 119 metrology reactions with covariance information and corresponding decay data. The library also includes 4 cover cross sections of B, ^{10}B, Cd and Gd used to support self-shielding corrections, 5 metrology metrics used by the dosimetry community, and 7 cumulative fission products yields. Several reference neutron fields for library validation are also provided. Finally, recommended radionuclide masses and elemental abundances to be used for dosimetry applications are also included. The dosimetry library can be used in a broad range of applications from lifetime management and assessments of nuclear power reactors to other neutron metrology applications such as boron neutron capture therapy, therapeutic use of medical isotopes, nuclear physics measurements, and reactor safety applications. Library evaluations are based mainly on comprehensive experimental data, therefore the reaction library also represents an ideal benchmark collection for validation and improvement of theoretical nuclear reaction modelling. The older library release IRDFF-v1.05 is now superseded by the new IRDFF-II library but is still used on many instances in reactor dosimetry community. Figure 6 shows high-energy reaction ^{54}Fe(n,p) from three different cross section libraries, which were used in this paper. Figure 7 shows differences in reaction ^{238}U(n,f) between IRDFF evaluations, which are quite noticeable in the resonance region. Retrieval, formatting and data plotting was done using IAEA Nuclear Data Services available at: https://www-nds.iaea.org/. The special dosimetry libraries were manually added to MCNP/DATA directory, with necessary modification of the "xsdir" files, so library selection is done through argument "xsdir=..." in the MCNP command line.

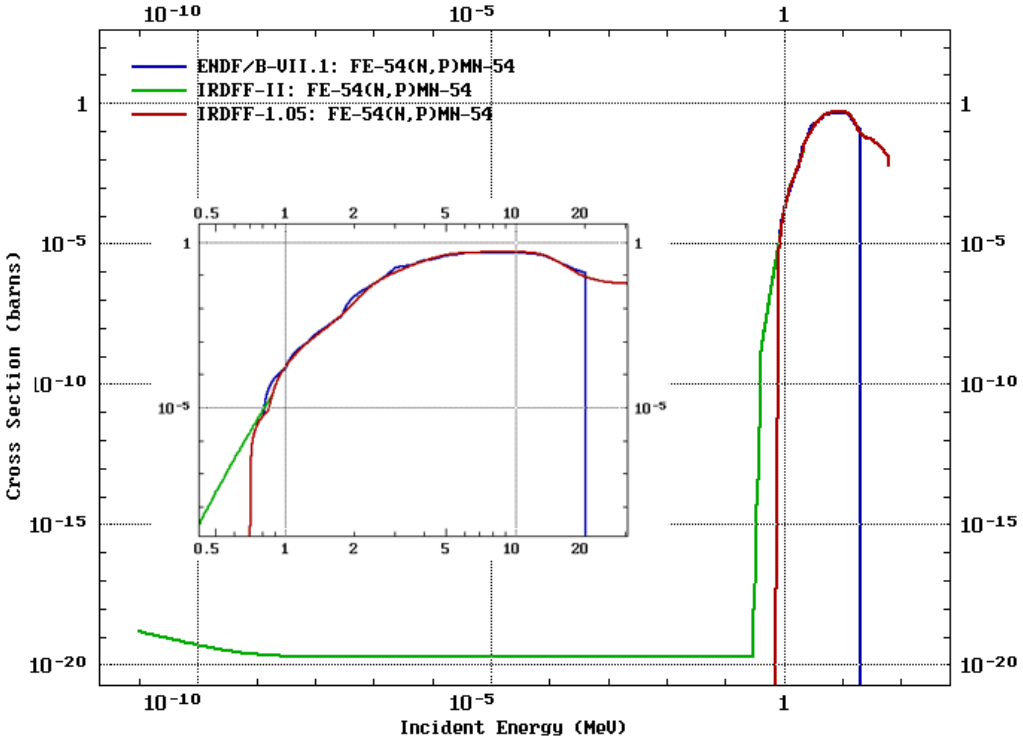

Figure 6: Comparison of reaction ^{54}Fe(n,p) from three different libraries

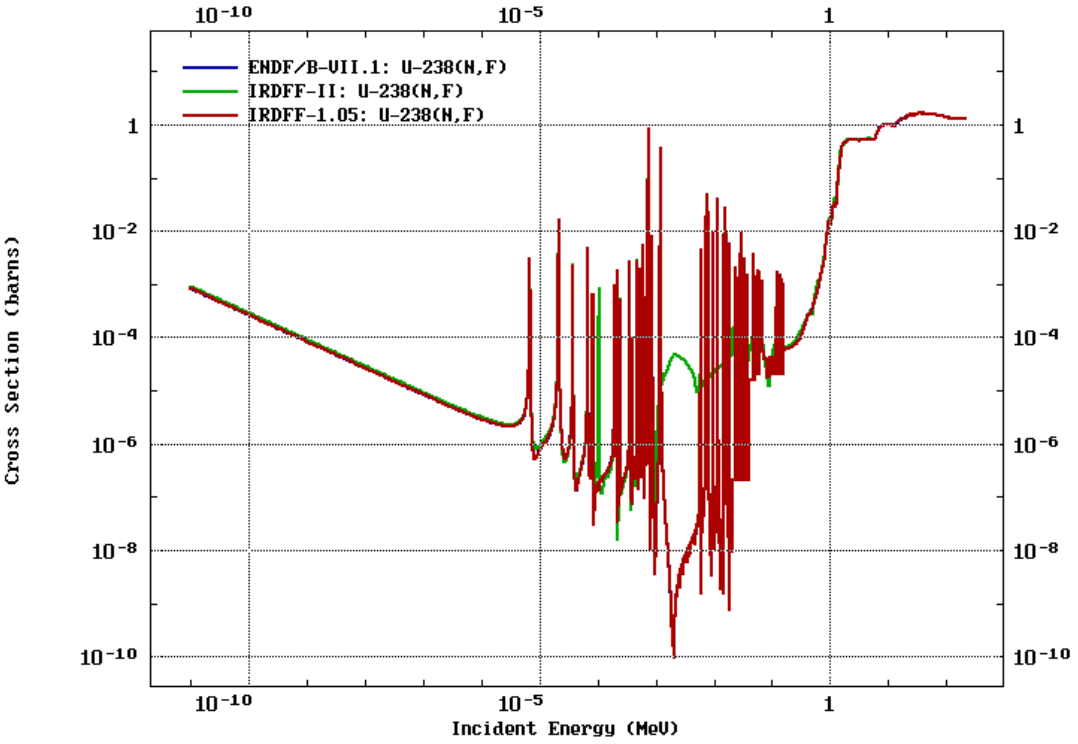

Figure 7: Comparison of reaction ^{238}U(n,f) from three different libraries (red covers blue)

4 RESULTS AND DISCUSSION

The mesh tally distribution of the fast neutron flux emerging in ambient air around the iron sphere is shown in Figure 8 together with MC relative errors. One can notice axial path of neutron streaming throughout the rabbit system which is not affecting point detector tally solution but has a marginal impact on the surface flux tally and the cell flux tally, since average neutron flux over those objects is increased. The neutron flux distribution as a function of x-axis is depicted in Figure 9, together with associated relative errors, which show steady increase up to 2% on average at detector location (r=100 cm). It is interesting to notice a change in the relative error curve profile from an exponential growth inside the iron sphere, due to strong attenuation, to a linear growth outside the sphere. The total point detector flux was found to be $7.85631 \cdot 10^{-6} \pm 0.44\%$, and after multiplying it with source intensity (125664 n/s) one obtains proper normalized value of 0.987. The total surface flux over a sphere tally with r=100 was found to be $7.8913 \cdot 10^{-6} \pm 0.00\%$. These results clearly show uniform MC convergence so additional results follow.

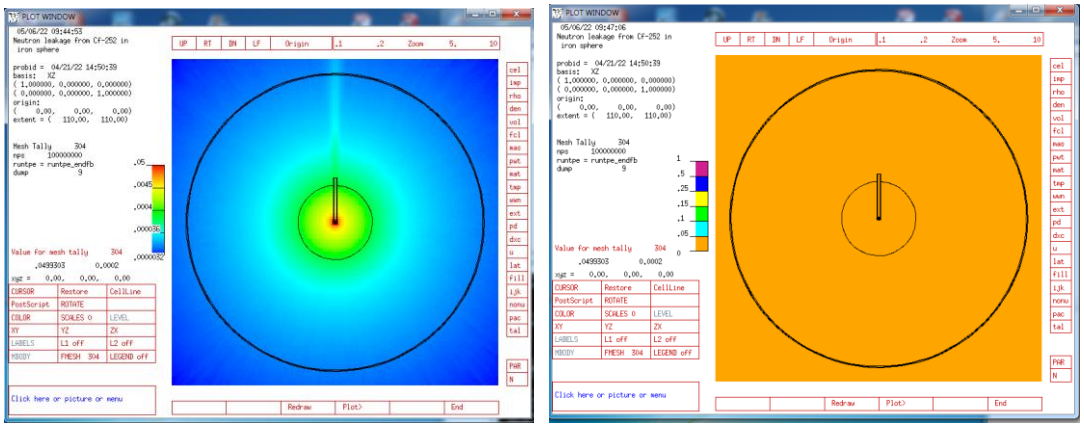

Figure 8: Mesh tally of neutron flux in y=o plane with relative errors

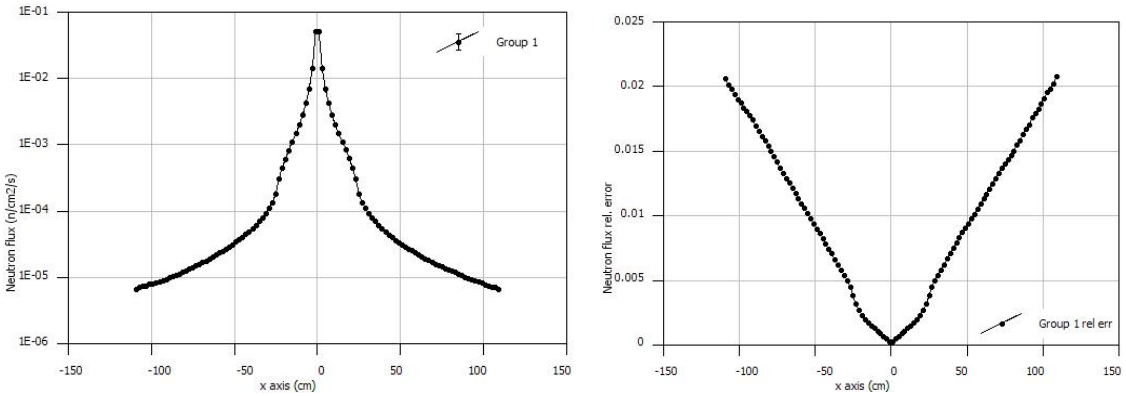

Figure 9: Neutron flux as a function of radial distance with rel. errors in x-axis

The calculated MCNP full neutron leakage spectrum is plotted in Figure 10 in comparison with the referenced one [1], while high-energy part above 1 keV is shown in Figure 11. Below 1 keV one can notice 1/E slowing down tail. A generally good agreement is obtained between MCNP and referenced results over entire spectrum domain, considering that local difference in curve variations are due to different tally energy group structure representation. However, above 1 MeV region, the spectrum solution based on ENDF/B-VII.1 evaluation shows overall higher values compared to an older ENDF/B-VI evaluation. This means that improvement in ENDF/B-VI iron data evaluation, which was first reported in [1], is also present in the ENDF/B-VII.1 iron data in predicting neutron transmission above 1 MeV. A rough assessment can be made that the same fast

flux ratio of ENDF/B-VI to ENDF/B-V is also present in ratio ENDF/B-VII.1 to ENDF/B-VI evaluation. Since high-energy tail of the neutron spectrum is affecting at most high-energy dosimetry reactions, it is expected that largest difference in dosimeter reaction rates will be for reactions ^{63}Cu(n,α), ^{54}Fe(n,p) and ^{58}Ni(n,p) (see Table 1 for reaction thresholds).

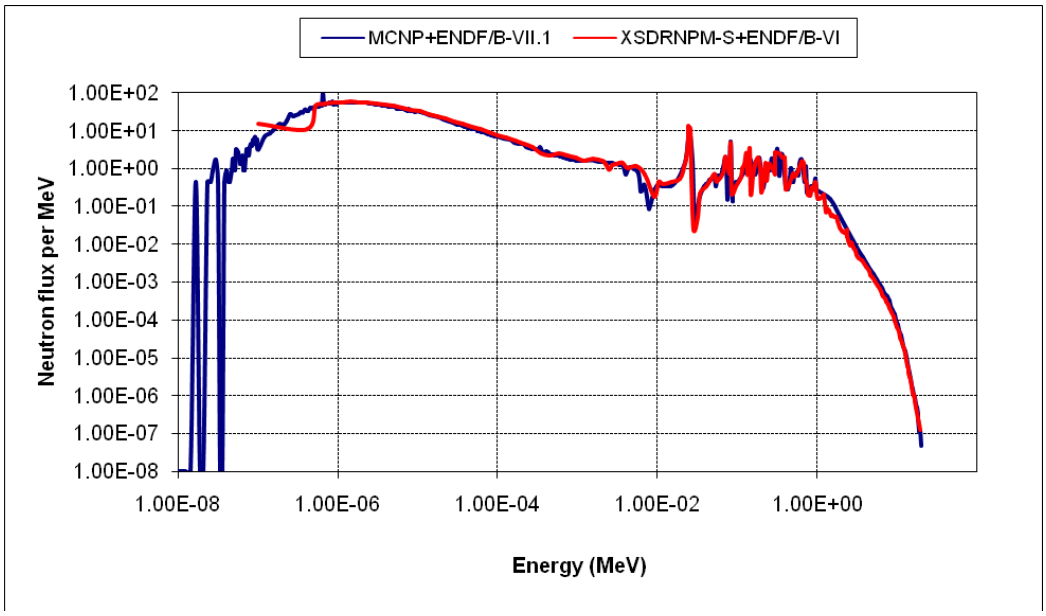

Figure 10: Comparison of fast neutron leakage spectra in point detector

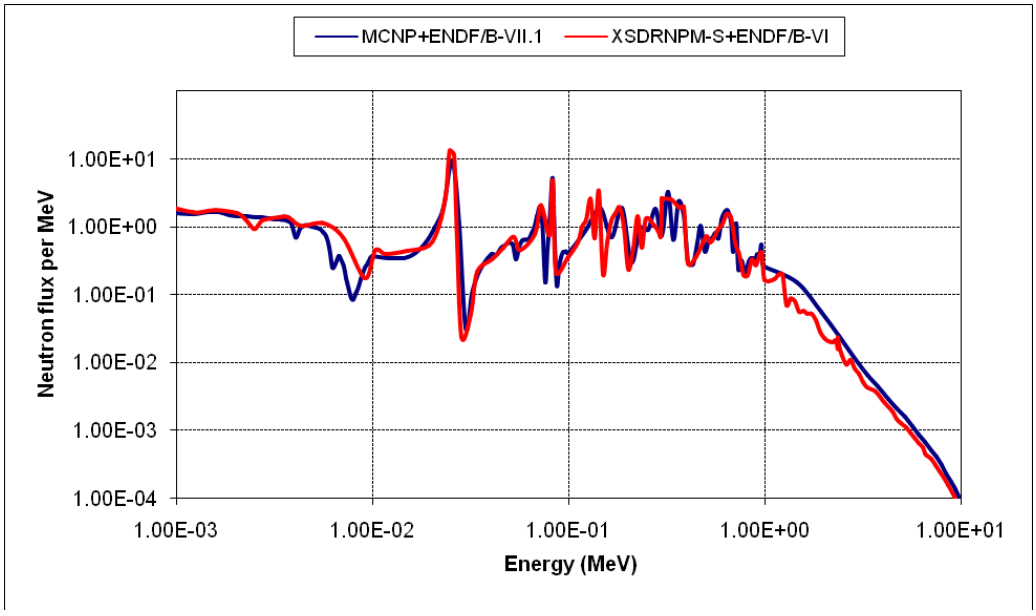

Figure 11: High-energy detail of the neutron leakage spectra above 1 keV

The comparison of point detector fast neutron flux based on ENDF/B-VII.1 iron evaluation and its relative ratio to previous ENDF/B-VI evaluation is shown in Table 2 for different energy intervals. The total flux on point detector was $7.85631 \cdot 10^{-6} \pm 0.02\%$, and its mean value was used to calculate relative intensities over energy intervals. One can notice similar values for the ratios, so it is evident that fast neutron transmission in iron is even more augmented in the ENDF/VII.1 evaluation (in absolute sense). Even thought differences do exist between reaction cross sections from special dosimetry libraries, one must bear in mind that calculated dosimeter activities represent integral energy quantities, so detector activities should be similar. Tables 3, 4 and 5

present detector reaction rates based on response functions taken from different libraries (ENDF/B-VII.1, IRDFF-1.05 and IRDFF-II) and comparison with original values based on VITAMIN-E dosimetry library. Overall increase in all reaction rates can be seen as a direct consequence of higher neutron transmission in ENDF/B-VII.1 transport library (above 1 MeV). The results based on IRDFF-II should be taken as relevant ones, since this library is latest and recommended by IAEA Nuclear Data Bank.

Table 2: Detector fast neutron flux obtained using ENDF/B-VII.1 transport cross sections

Flux range	Response per source particle (neutron/cm^2*s)	Ratio ENDF/B-VI to ENDF/B-V	Response per source particle (neutron/cm^2*s)	Ratio ENDF/B-VII.1 to ENDF/B-VI
> 0.1 MeV	$8.82750 \cdot 10^{-1}$	0.996	$(7.09264 \cdot 10^{-6} \pm 0.02\%)$ $9.02799 \cdot 10^{-1}$	1.023
> 1.0 MeV	$1.05200 \cdot 10^{-1}$	1.095	$(9.86505 \cdot 10^{-7} \pm 0.05\%)$ $1.25568 \cdot 10^{-1}$	1.194
> 2.0 MeV	$2.09600 \cdot 10^{-2}$	1.173	$(2.02110 \cdot 10^{-7} \pm 0.14\%)$ $2.57258 \cdot 10^{-2}$	1.227
> 3 MeV	$7.28900 \cdot 10^{-3}$	1.289	$(7.33235 \cdot 10^{-8} \pm 0.27\%)$ $9.33307 \cdot 10^{-3}$	1.280
> 4 MeV	$3.45200 \cdot 10^{-3}$	1.341	$(3.66788 \cdot 10^{-8} \pm 0.44\%)$ $4.66871 \cdot 10^{-3}$	1.353

Table 3: Detector reaction rates obtained using ENDF/B-VII.1 transport cross sections (response functions taken from general ENDF/B-VII.1 library)

Reaction	Response per source particle (reaction/atom*s)	Ratio ENDF/B-VI to ENDF/B-V	Response per source particle (reaction/atom*s)	Ratio ENDF/B-VII.1 to VITAMIN-E
63Cu(n,α)	$1.55919 \cdot 10^{-34}$	1.216	$2.1700 \cdot 10^{-34} \pm 0.42\%$	1.392
54Fe(n,p)	$2.15592 \cdot 10^{-32}$	1.229	$3.2354 \cdot 10^{-32} \pm 0.21\%$	1.500
58Ni(n,p)	$3.52498 \cdot 10^{-32}$	1.184	$4.9932 \cdot 10^{-32} \pm 0.17\%$	1.417
238U(n,f)	$1.93676 \cdot 10^{-31}$	1.106	$2.5149 \cdot 10^{-31} \pm 0.08\%$	1.299
237Np(n,f)	$3.89389 \cdot 10^{-30}$	1.039	$4.4012 \cdot 10^{-30} \pm 0.03\%$	1.130
59Co(n,g)	$3.88028 \cdot 10^{-31}$	1.267	$4.5507 \cdot 10^{-31} \pm 1.25\%$	1.173

Table 4: Detector reaction rates obtained using ENDF/B-VII.1 transport cross sections (response functions taken from special IRDFF-1.05 library)

Reaction	Response per source particle (reaction/atom*s)	Ratio ENDF/B-VI to ENDF/B-V	Response per source particle (reaction/atom*s)	Ratio IRDFF-1.05 to VITAMIN-E
63Cu(n,α)	$1.55919 \cdot 10^{-34}$	1.216	$2.2125 \cdot 10^{-34} \pm 0.41\%$	1.419
54Fe(n,p)	$2.15592 \cdot 10^{-32}$	1.229	$3.0955 \cdot 10^{-32} \pm 0.23\%$	1.436
58Ni(n,p)	$3.52498 \cdot 10^{-32}$	1.184	$4.7655 \cdot 10^{-32} \pm 0.18\%$	1.352
238U(n,f)	$1.93676 \cdot 10^{-31}$	1.106	$2.5135 \cdot 10^{-31} \pm 0.08\%$	1.298
237Np(n,f)	$3.89389 \cdot 10^{-30}$	1.039	$4.4274 \cdot 10^{-30} \pm 0.03\%$	1.137
59Co(n,g)	$3.88028 \cdot 10^{-31}$	1.267	$4.4451 \cdot 10^{-31} \pm 0.93\%$	1.146

Table 5: Detector reaction rates obtained using ENDF/B-VII.1 transport cross sections (response functions taken from special IRDFF-II library)

Reaction	Response per source particle (reaction/atom*s)	Ratio ENDF/B-VI to ENDF/B-V	Response per source particle (reaction/atom*s)	Ratio IRDFF-II to VITAMIN-E
63Cu(n,α)	$1.55919 \cdot 10^{-34}$	1.216	$2.2125 \cdot 10^{-34} \pm 0.41\%$	1.419
54Fe(n,p)	$2.15592 \cdot 10^{-32}$	1.229	$3.0953 \cdot 10^{-32} \pm 0.23\%$	1.436
58Ni(n,p)	$3.52498 \cdot 10^{-32}$	1.184	$4.7653 \cdot 10^{-32} \pm 0.18\%$	1.352
238U(n,f)	$1.93676 \cdot 10^{-31}$	1.106	$2.5790 \cdot 10^{-31} \pm 0.08\%$	1.332
237Np(n,f)	$3.89389 \cdot 10^{-30}$	1.039	$4.4385 \cdot 10^{-30} \pm 0.03\%$	1.140
59Co(n,g)	$3.88028 \cdot 10^{-31}$	1.267	$4.4450 \cdot 10^{-31} \pm 0.93\%$	1.146

5 CONCLUSION

Transport calculations of RPV fluence have indicated in the past underestimation of the dosimeter activities when using cross sections based on the ENDF/B-IV or ENDF/B-V evaluations [1]. The paper from Sajo et al [1] compares results of transport calculations based on ENDF/B-V and ENDF/B-VI evaluations, in relation to experimentally measured data for iron sphere. It was shown that for neutron energies above 1 MeV, ENDF/B-VI iron cross sections yield an increased neutron penetration through steel compared to calculations based on the ENDF/B-V. Moreover, it was noticed that the high-energy responses change by the greatest amount. The conclusion was how the ENDF/B-VI cross sections, even though improved, will not entirely resolve spectrum underestimation above 1 MeV relative to experimental data, so further refinement in iron data and/or ^{252}Cf neutron spectrum is needed.

This paper presents continuation of this work using the MCNP code based on transport cross sections from ENDF/B-VII.1 evaluation, containing updated neutron inelastic data. The obtained fast neutron flux and detector reaction rates confirmed increased neutron transmission in iron over energies above 1 MeV, compared to SN results based on ENDF/B-VI evaluation. The point detector results were verified with other tally objects, while MCNP neutron leakage spectra showed a good agreement with a reference case, except for energies above 1 MeV where it is larger on the average. This at the end produced higher reaction rates on detector by 30% to 40% for high energy threshold reactions ^{63}Cu(n,α), ^{54}Fe(n,p) and ^{58}Ni(n,p). For other reactions ^{238}U(n,f), ^{237}Np(n,f) and ^{59}Co(n,g) this increment declined to values 14% to 30%. All reactions were taken from the recommended IRDFF-II dosimetry library and produce almost the same results as reactions from IRDFF-1.05.

In addition to using the standard reaction cross section data from neutron transport libraries, MCNP provides dosimetry or activation reaction data that can be used as a response function in calculating energy integral of $\sigma(E)\phi(E)$, where $\sigma(E)$ is the microscopic cross section and $\phi(E)$ is the neutron flux. The dosimetry data libraries are appropriate only when used as a source of $\sigma(E)$ for "FM" tally multipliers, so they can't be used as a material data source for neutron transport. For this study, special dosimetry libraries IRDFF-1.05 and IRDFF-II were added to MCNP/DATA directory, replacing older built-in dosimetry data. Continuation of this work with MCNP will test the latest iron ENDF/B-VIII.0 evaluation for fast neutron transmission.

REFERENCES

[1] E. Sajo, M.L. Williams, M. Asgari, "Comparison of measured and calculated neutron transmission through steel for a ^{252}Cf cource," Annals of Nuclear Energy, Vol. 20, No. 9, pp. 585-604, 1993.

[2] M.L. Williams et al, "Transport calculations of neutron transmission through steel using ENDF/B-V, revised ENDF/B-V and ENDF/B-VI iron evaluations," Annals of Nuclear Energy, Vol. 18, No. 10, pp. 549-565, 1991.

[3] M.B. Chadwick, M. Herman, P. Obložinsky, et al., "ENDF/B-VII.1: ENDF/B-VII.1: Nuclear Data for Science and Technology: Cross Sections, Covariances, Fission Product Yields and Decay Data", Nuclear Data Sheets, Vol. 112(2011)2887.

[4] A. Trkov, P.J. Griffin, S.P. Simakov, L.R. Greenwood, K.I. Zolotarev, R. Capote, D.L. Aldama, V. Chechev, C. Destouches, A.C. Kahler, C. Konno, M. Kostal, M. Majerle, E. Malambu, M. Ohta, V.G. Pronyaev, V. Radulovic, S. Sato, M. Schulc, E. Simeckova, I. Vavtar, J. Wagemans, M. White, and H. Yashima, IRDFF-II: A New Neutron Metrology Library. Special issue of Nuclear Data Sheets, Vol. 163, pp. 1-108 (2020).

[5] R. Capote, K.I. Zolotarev, V.G. Pronyaev, and A. Trkov, International Reactor Dosimetry and Fusion File IRDFF v.1.05, 09 October 2014, J. ASTM International, Volume 9, Issue 4, April 2012, JAI104119

[6] T. M. Evans, A. S. Stafford, R. N. Slaybaugh, K. T. Clarno, "Denovo: A New Three-Dimensional Parallel Discrete Ordinates Code in SCALE", Nuclear Technology, 171, 2010, pp. 171-200.

[7] J.C.Wagner and A. Haghighat, "Automated variance reduction of Monte Carlo shielding calculations using the discrete ordinates adjoint function," Nuclear Science and Engineering, Vol. 128, no. 2, pp. 186–208, 1998.

[8] S.W. Mosher, S.R. Johnson, A.M. Bevil et al., "ADVANTG – An Automated Variance Reduction Parameter Generator," ORNL/TM-2013/416, Rev. 1, August 2015.

[9] G. I. Bell, S. Glasstone, "Nuclear Reactor Theory", Van Nostrand Reinhold Company, New York, 1970.

[10] E. E. Lewis, W. F. Jr. Miller, "Computational Methods of Neutron Transport", American Nuclear Society, Illinois, 1993.

[11] T. Goorley, "MCNP6.1.1-Beta Release Notes," LA-UR-14-24680, 2014.

[12] "VisIt: An End-User Tool for Visualizing and Analyzing Very Large Data", Lawrence Livermore National Laboratory, VisIt Getting Started Manual, February 2003, UCRL-MA-148506-REV-1, Version 2.7.3.

[13] IAEA Nuclear Data Services. Website: https://www-nds.iaea.org/.